Energy Trap for Axial-Shear-Wave Resonance in a Stepped Cylindrical Rod: Theory and Measurement

Hirotsugu Ogi, Kayo Wada, and Masahiko Hirao
Graduate School of Engineering Science, Osaka University, 1-3 Machikaneyama, Toyonaka, Osaka 560-8531, Japan

Methodology to trap the vibrational energy of axially polarized surface-shear wave (axial-shear wave) in a stepped cylindrical rod is presented. Central part of the rod had slightly larger diameter where the resonance vibration was trapped. Magnetostriction effect of steel allowed us to generate and detect the resonance with noncontacting. An approximated analysis derived a resonance equation and displacement distribution of trapped axial-shear-wave modes. The displacement was measured along the axial direction, which exponentially decreased with the distance from the center. This trend agreed with the theoretical calculation.

KEYWORDS: energy trap, electromagnetic acoustic transducer, magnetostriction, noncontacting measurement, surface-shear wave

1. Introduction

Free-vibration resonance frequencies of a solid (or resonator) is changed by a contact with another material depending on the mass, elasticity, and electric properties of the contacting material. Thus, measuring resonator's resonance frequencies allows one to detect such properties of the contacting material. This principle is applicable to gas sensors [1], gyro sensors [2], bio-chemical sensors [3], and elastic-constant mapping [4-6]. Developing a sensitive, temperature-stable, and high-efficient resonator has been a long-running topic. Tow demands to achieve this appear every time; they are (i) trapping of vibrational energy and (ii) noncontacting measurement. All acoustic resonators must be mechanically supported and if vibrational amplitudes are significant at the points of contact, there is a leakage of acoustic energy into the supporting structure, which causes a decrease in Q. Also, electrodes deposited on a resonator material affects its vibrations and they sometimes significantly deteriorate resonator's sensing ability.

This study proposes methodology to excite and detect surface-shear-horizontal-wave resonance in a ferromagnetic rod with noncontacting and to trap its vibrational energy in the rod. An electromagnetic field applied to a ferromagnetic material can cause ultrasonic vibrations via the magnetostriction response [7]. Here, we use an electromagnetic acoustic transducer (EMAT) [8] to generate and detect the axial-shear wave in a steel rod.

Johnson *et al*. [9] showed that torsional vibrations can be trapped in a stepped rod so as

to use such a mode that shows an imaginary wavenumber outside the steps. They gave an approximated theory to calculate the resonance frequencies and displacement distribution of the trapped torsional modes. Following their work, we intend to trap vibrational energy of axial-shear-wave resonances between the steps.

2. Trap Modes of Axial-Shear Wave

An axially polarized shear wave, called axial shear wave, travels in the circumferential direction along a cylindrical surface of a circular rod or pipe specimen [10, 11]. First, we consider axial-wave resonances in a non-stepped (usual) cylinder rod. Considering only the nonzero axial displacement in a r-θ-z cylindrical coordinate system, where the z-axis is along cylinder's axial direction, equation of motion yields the displacement u_z of axial-shear wave of the form:

$$u_z = \left(C_1 \mathrm{e}^{\mathrm{j}p\kappa z} + C_2 \mathrm{e}^{\mathrm{j}p\kappa z}\right) J_n\left(\tilde{\eta}_n r/a\right) \mathrm{e}^{\mathrm{j}(\omega t + n\theta)}, \tag{1}$$

where

$$\kappa^2 = \left(\frac{\omega}{v_s}\right)^2 - \left(\frac{\tilde{\eta}_n}{a}\right)^2. \tag{2}$$

Here, C_1 and C_2 are arbitrary constants. a denotes the cylinder radius, J_n the nth Bessel function of the first kind, ω the angular frequency, and v_s the shear-wave velocity. $p = \sqrt{\mu/(\lambda + 2\mu)}$ is given by Lamé's constants λ and μ. Integer n represents half node number in the circumferential direction. $\tilde{\eta}_n$ denotes the normalized wavenumber along the

radial direction and satisfies the boundary condition of the zero stress (σ_{rr}=0) on the outer surface:

$$nJ_n(\tilde{\eta}_n) - \tilde{\eta}_n J_{n+1}(\tilde{\eta}_n) = 0\,. \tag{3}$$

κ=0 gives the cutoff frequency $\omega_0 (= \tilde{\eta}_n v_s / a)$. Frequencies below ω_0 provide imaginary values of κ and non-propagating modes, which decay with distance from the origin along the *z* axis.

Second, we consider a stepped cylinder that has a slightly smaller radius *a*' outside the central region with radius *a* (>*a*') as shown in Fig. 1. Axial length of the central region is 2*l*. Assuming a common $\tilde{\eta}_n$ through the steps, the cutoff frequencies differ from each other at the two regions. Let them be ω_0 and ω_0', respectively. (Johnson *et al*. [9] proved experimentally for torsional modes that this assumption is allowable when the radius mismatch is sufficiently small.) Figure 2 shows dispersion curves calculated near cutoff for the two regions for a standard steel rod with *a*=7 mm and *a*'=6.875 mm. Note that the frequencies between ω_0 and ω_0' will provide real values of κ in the central region and imaginary values of κ in the outside region, indicating that the displacement of such a resonance mode decreases exponentially with distance from the center in the outside region to remain finite at $z \to \pm\infty$. Thus, the resonance vibration can be trapped at the central region with larger radius.

We consider only symmetric modes about the z axis because of the EMAT configuration shown later. The displacements u_z and u'_z in the central and outside regions, respectively, are

$$u_z = 2C_1 \cos(p\kappa z) J_n(\tilde{\eta}_n r/a) e^{j(\omega t + n\theta)}, \tag{4}$$

$$u'_z = C_3 e^{-p|\kappa'|z} J_n(\tilde{\eta}_n r/a') e^{j(\omega t + n\theta)}, \tag{5}$$

when $z>0$. Here, C_3 is a constant and κ' is given by Eq. (2) with a' instead of a. Continuity for displacements and three stress components σ_{zz}, σ_{zr}, and $\sigma_{z\theta}$ are required at the step boundary ($z=l$). However, because no analytical solution achieves these requirements simultaneously at every point on the cross-section, we use the weak forms for the boundary conditions. For example,

$$\int_0^a u_z dr = \int_0^{a'} u'_z dr \quad \text{and} \quad \int_0^a \sigma_{zz} dr = \int_0^{a'} \sigma'_{zz} dr \quad \text{at} \quad z=l. \tag{6}$$

Equations (1) and (6) yields

$$\frac{\kappa}{|\kappa'|} \tan(p\kappa l) = 1. \tag{7}$$

The weak form for the σ_{zr} continuity and continuity of $\sigma_{z\theta}$ are reduced to the same form as the weak form for displacement continuity. Thus, Equation (7) determines the resonance frequencies of symmetric trapped axial-shear-wave modes and we can calculate their displacement distributions by Eqs. (4) and (5). The validity of adopting the weak forms are

confirmed experimentally as shown later.

Figure 3 shows the surface-displacement distributions of the lowest trapped axial-shear-wave mode calculated in three steel rods with a=7 mm and l=15 mm for (a−a')/a=0.10, 0.36, and 1.79%. The displacements are well trapped in the central region and they rapidly decay with the distance from the center in the outside region. A larger step achieves higher degree of energy concentration. We note that a very small radius mismatch (~0.10%) can trap the surface wave in the central region.

3. Measurements

We used a meander-line coil EMAT shown in Fig. 4 to excite and detect the trapped axial-shear-wave resonance with noncontacting and to verify the approximation theory above. The EMAT consists of a meander-line coil to induce the dynamic field in the circumferential direction. A static field $\mathbf{H}_0$ is applied along the axial direction (Fig. 1). When a sinusoidal current is applied to the meander-line coil to induce the dynamic field $\mathbf{H}_\omega$ along the circumferential direction, the total field $\mathbf{H}_t$ oscillates about the axial direction at the same frequency as the driving current and produces shearing vibration through the magnetostrictive effect to excite the axial shear wave propagating along the circumference with axial polarization. The meander-line coil also receives the axial shear wave through the reverse magnetostrictive effect. This noncontacting acoustic-coupling mechanism is explained in

detail elsewhere [7, 8]. Received signals were entered to a superheterodyne spectrometer to detect the same frequency component of amplitude as the driving frequency [8]. A frequency scan provides a resonance spectrum. Representative resonance spectrum of the axial-shear-wave resonance appear elsewhere [12].

The specimen was 0.45mass%C steel rod with a=7 mm, a'=6.875 mm, and l=15 mm. The meander-line period δ was 0.9 mm, which determines n to be n=49 via $n \approx 2\pi a/\delta$ [11]. Axial length of the coil was 20 mm. Because the central part of the meander-line coil was located at z=0, the resulting displacement of axial-shear-wave mode is symmetric about z. The biasing magnetic field was 2.0×10^3 A/m.

To measure the displacement distribution along the z axis, we used a pinducer which possesses a needle to contact the specimen surface (see Fig. 1). (Because the axial-shear-wave modes show zero out-of-plane displacement, standard laser measurements were unavailable.) We applied a normal biasing force to the pinducer to detect the in-plane deformation via a frictional contact. Driving the EMAT with the measured resonance frequency, we detected the displacement amplitude by the pinducer. We measured the maximum displacement along the circumferential direction at each axial position because the displacement depends on θ. The meander-line coil with 20-mm width prevented us from measuring the displacement in the region $z<10$ mm.

4. Results and Discussion

The shear-wave velocity v_s is needed to calculate the resonance frequency of a trapped axial-shear-wave mode. We determined this to be v_s=3218.5 m/s by measuring the resonance frequency of the non-stepped steel rod of 7-mm radius obtained from the same material as the specimen: its resonance frequency can be exactly calculated by Eq. (3).

The lowest resonance frequency of the trapped axial-shear-wave mode for n=49 calculated using Eq. (7) is 3.8048 MHz, which agrees well with the measured resonance frequency 3.8058 MHz by 0.03%, highly indicating the validity of the approximated theory.

Figure 5 compares the measured displacement distribution with the calculation. (Note that logarithmic scale is used for the vertical axis.) Measurement on the non-stepped steel rod is also shown for comparison. Clearly, the axial-shear-wave energy is trapped at the central region in the stepped rod: the displacement exponentially decays outside the step. The theory successfully explains this trend. Thus, the approximated theory above is applicable to the axial-shear-wave resonance in a stepped rod when $\Delta a/a$ is small. The displacement amplitude is decreased almost to noise level within 5 mm outside from the step.

5. Conclusion

We have presented a surface-shear-wave resonator excited with noncontacting via the magnetostriction effect. The vibrational energy is efficiently trapped at a central part of a

cylindrical rod, where the diameter is slightly larger. An approximated model for the trapped axial-shear-wave mode is presented, which showed good agreement with measurements. Because this resonator requires no electrodes on the material and can be supported without disturbing the vibration, it can be a candidate for high-sensitive acoustic sensor. This study used the biasing magnetic field, but it will be nonnecessity by replacing steel with other ferromagnetic materials showing larger magnetostriction, such as nickel or giant magnetostriction materials.

References

[1] S. Okuyama, Y. Mitobe, K. Okuyama, and K. Matsushita: Jpn. J. Appl. Phys. **39** (2000) 3584.

[2] H. Tamura, Y. Tomikawa, T. Kikuchi, and S. Sugawara: Jpn. J. Appl. Phys. **37** (1998) 2859.

[3] H. Muramatsu, J. Dicks, E. Tamiya, and I. Karube, Anal. Chem. **59** (1987) 2760.

[4] K. Yamanaka, H. Ogiso, O. Kolosov, Appl. Phys. Lett. **64**, (1994) 178.

[5] O. Wright, N. Nishiguchi, Appl. Phys. Lett. **71**, (1997) 626.

[6] H. Ogi, J. Tian, T. Tada, and M. Hirao, Appl. Phys. Lett. **83** (2003) 464.

[7] H. Ogi, E. Goda, and M. Hirao, Jpn. J. Appl. Phys. **42** (2003) 3020.

[8] M. Hirao and H. Ogi, EMATs for Science and Industry: Noncontacting Ultrasonic Measurements (Kluwer Academic, Boston, 2003).

[9] W. Johnson, B. Auld, and E. Segal, J. Acoust. Soc. Am. **100** (1996) 285.

[10] W. Johnson, B. A. Auld, and G. A. Alers, Review of Progress in QNDE, edited by D. O. Thompson and D. E. Chimenti (Plenum, New York, 1994) Vol. 13, p. 1603.

[11] H. Ogi, Y. Minami, and M. Hirao, J. Appl. Phys. **90**, (2002) 438.

[12] H. Ogi, T. Hamaguchi, and M. Hirao, Metal. Mater. Trans. **31A** (2000) 1121.

Figure captions

Fig. 1 Measurement setup for the displacement distribution along the axial direction of the stepped steel rod.

Fig. 2 Dispersion curves of steel rods of radii 7 and 6.875 mm.

Fig. 3 Normalized surface displacements on stepped steel rods with various radius mismatches $\Delta a=a-a'$ at the step.

Fig. 4 Magnetostrictive excitation of the axial-shear wave by a meander-line coil and axial static magnetic field.

Fig. 5 Calculated and measured surface displacement on the stepped (a=7 mm and a'=6.875 mm) and non-stepped steel rods (a=7 mm).

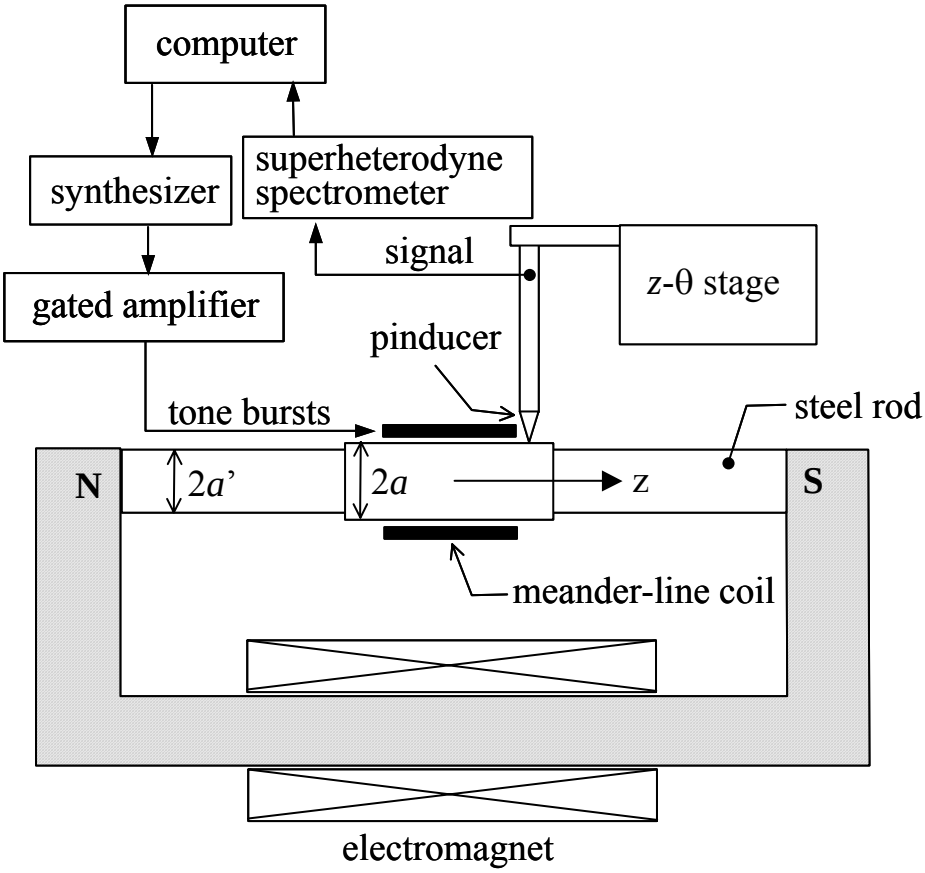
computer
synthesizer
superheterodyne
spectrometer
signal
z-θ stage
gated amplifier
pinducer
tone bursts
steel rod
N
2a'
2a
z
S
meander-line coil
electromagnet

Fig.1

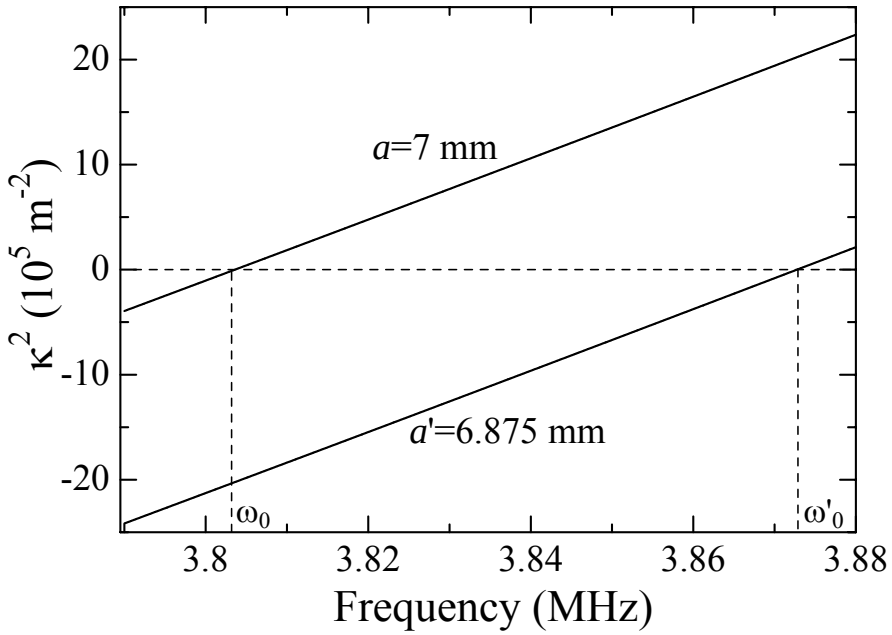
20
10
0
-10
-20
κ^2 (10^5 m^{-2})
a=7 mm
a'=6.875 mm
ω_0
ω'_0
3.8
3.82
3.84
3.86
3.88
Frequency (MHz)

Fig. 2

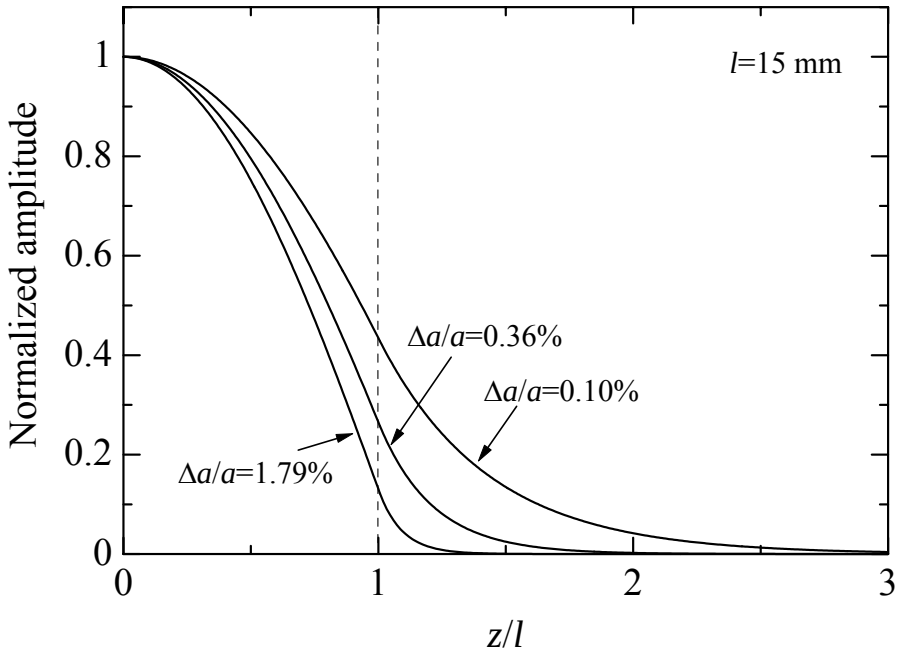
Normalized amplitude
z/l
l=15 mm
Δa/a=0.36%
Δa/a=0.10%
Δa/a=1.79%
0
0.2
0.4
0.6
0.8
1
0
1
2
3

Fig. 3

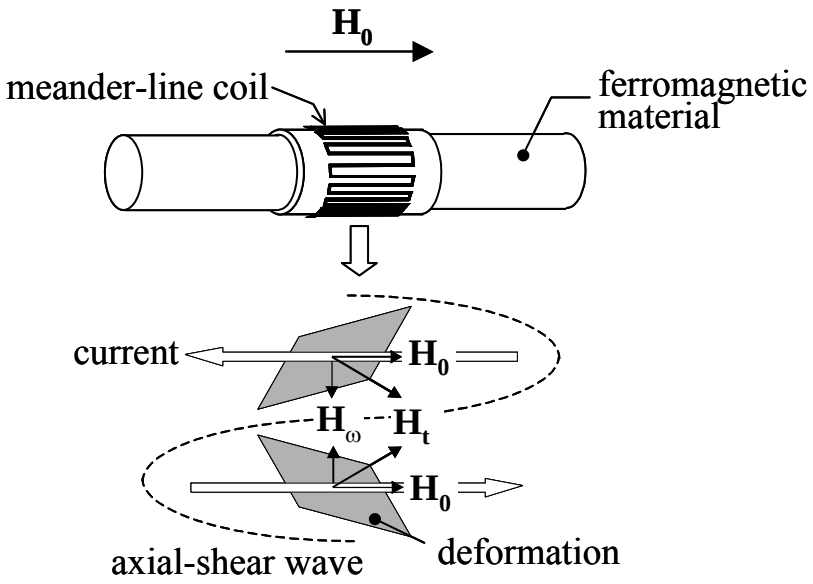
H0
meander-line coil
ferromagnetic material
current
H0
Hω
Ht
H0
axial-shear wave
deformation

Fig. 4

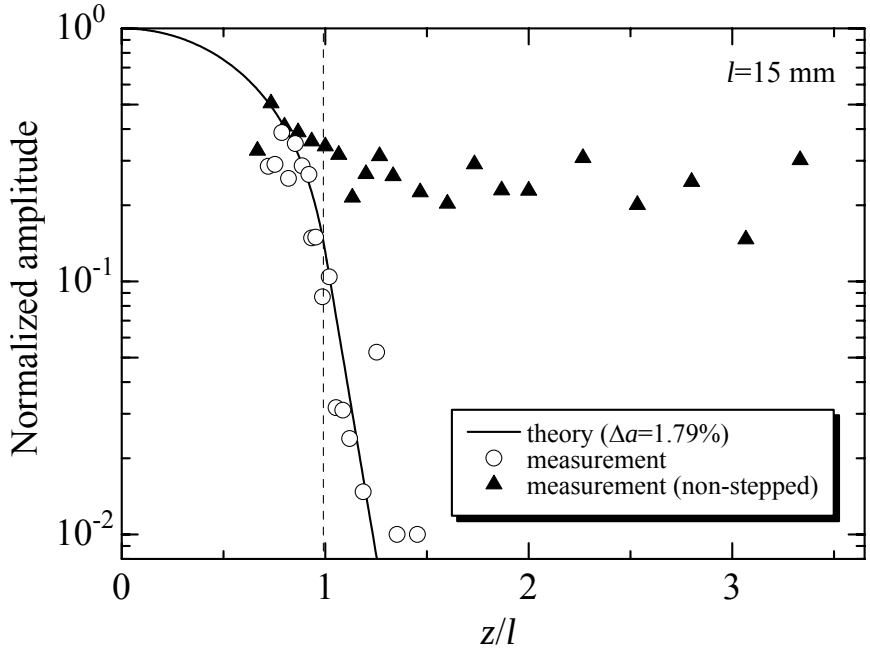
10^0
10^{-1}
10^{-2}
Normalized amplitude
l=15 mm
theory (Δa=1.79%)
measurement
measurement (non-stepped)
0
1
2
3
z/l

Fig. 5